IEEE Photonics Journal
An IEEE Photonics Society Publication

Open Access

Experimental Demonstration of an LCoS-Based Access Node for Bidirectional Optical Wireless Communications

Volume 10, Number 4, August 2018

Hsi-Hsir Chou
Jen-Hao Hsiao

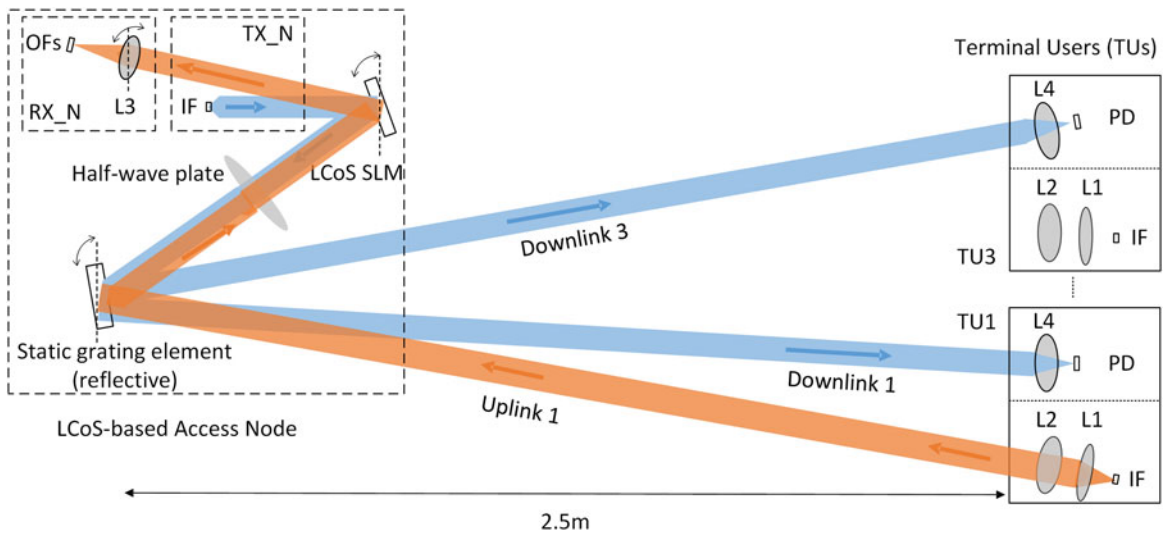

DOI: 10.1109/JPHOT.2018.2841395
1943-0655

Experimental Demonstration of an LCoS-Based Access Node for Bidirectional Optical Wireless Communications

Hsi-Hsir Chou and Jen-Hao Hsiao

Department of Electronic and Computer Engineering, National Taiwan University of Science and Technology, Taipei 106, Taiwan

DOI:10.1109/JPHOT.2018.2841395

Manuscript received May 8, 2018; revised May 21, 2018; accepted May 24, 2018. Date of publication June 1, 2018; date of current version June 21, 2018. This work was supported in part by the Ministry of Science and Technology (MOST), Taiwan (MOST 106-2221-E-011-011 and MOST 104-2221-E-011-046). Corresponding author: Hsi-Hsir Chou (e-mail: hsi-hsir.chou@trinity.cantab.net).

Abstract: An liquid crystal on silicon (LCoS)-based access node using optical fibers as the transmitter and receiver to deliver high-speed data transmission is proposed and experimentally demonstrated. This access node can be applied to a variety of networks ranging from passive optical networks to indoor home area networks through optical wireless communications without optical/electrical/optical (O/E/O) conversions. The link of system, which operates over ∼2.5 m with a possible wide field-of-view of nearly 97°, has been achieved through the implementation of a LCoS-based spatial light modulator in conjunction with a static grating element. A bidirectional optical wireless communication system was established to demonstrate the concept and evaluate the performance of the proposed access node, which uses typical WDM wavelengths (the channel spacing is 100 GHz) and is modulated at a data speed of more than 2.5 Gb/s. The results show that in downlink transmission, the multiple wavelengths delivered from optical fibers can be dynamically transmitted directly to the terminal users through the proposed access node architecture without performing any O/E/O conversion. Similarly in uplink transmission, all the wavelengths received at the proposed node architecture can be arbitrarily switched to a desired output fiber port of the access node to connect with the external fiber networks in the same manner. The bit error ratios of all the transmitted wavelengths in both uplink and downlink transmission scenarios are less than 10^{-9}.

Index Terms: Free-space optical communication, spatial light modulators, liquid crystal on silicon device.

1. Introduction

Next-generation Passive Optical Network Stage 2 (NG-PON 2) [1], [2] aims to provide high-speed data transmission rate over 10 Gbps and beyond, which has been proposed to fulfill the increasing bandwidth demand of multimedia services in home area networks (HANs). Efficient approaches for terminal users (TUs) to access these high-speed optical network services directly in HANs are thus highly interested due to the practical challenges of efficiently installing and using optical fibers arbitrarily. Although the technical solutions based on wireless access approaches may provide full mobility support for TUs, the major carrier frequencies of current wireless access technologies, i.e.,

Wi-Fi and WiMAX, are in microwave range as to limit the available modulation bandwidth. On the other hand, free-space optical wireless solutions have advantages of using unregulated free optical spectrum and providing immunity from electromagnetic interference. They are good alternative solutions to RF communications [3], [4] by extending high-speed optical fiber networks to indoor wireless networks.

In the development of optical wireless communication (OWC) technologies for HANs applications, direct line-of-sight (LOS) or diffused systems have been extensively studied [4], [5], most of them however still have shortages and limitations. It is noted that although the mobility support for TUs in HANs can be well provided through an indoor diffused system to optimize its performance by several advanced techniques, such as using angle diversity receiver [6], adaptive power and angle distribution techniques [7], [8], the performance improvement was found limited as exhibited by the recent experimental works in [9]. In addition to poor power efficiency, inter-symbol interference (ISI) and pulse spreading problems [6], [8] caused by multipath dispersions are also very severe.

To resolve these shortages, several technical solutions based on a LOS scenario have been developed to overcome the multipath dispersion and power consumption problems. However, these solutions are not able to provide mobility supports for TUs in HANs. Moreover, the alignment difficulties as well as the interruptions arising from physical shadowing during transmission also limit the applicability of LOS approaches in practical applications. Thus hybrid approaches using beam steering elements, i.e., MEMS (microelectromechanical systems) and LCoS (liquid crystal on silicon) devices were also examined to avoid the disadvantages in direct LOS approaches and diffused system [10], [11]. However, the mobility support is again limited because they were developed based on the communication scenarios of one-way transmission. It is further noted that although wavelength division multiplexing (WDM) transmission technology can be incorporated [10], [12] to maximize the channel capacity, the functionality of wavelength selection as well as the wavelength routing have not been well supported and investigated.

This study presents an experimental demonstration, for the first time to our best knowledge, of an LCoS-based access node (LCoS-AN) for indoor bidirectional optical wireless communication application [13]. In contrast to the work that has reported previously [13], the system level node architecture design is further presented and the system performance as well as the data transmission tests in uplink and downlink are thoroughly analyzed and evaluated. This experimental work is distinguished from conventional optical wireless communication systems [3]–[10] which are operated by a fixed point-to-point communication link, and may need several times of optical/electrical (O/E) and E/O conversions before the signals emit/couple from/into an optical fiber. In this work, the node architecture is implemented by using optical fibers as the transmitter and receiver for downlink and uplink transmissions, respectively. An LCoS-based SLM (LCoS-SLM) combining a static diffraction grating element is designed to achieve a wide field-of-view (FOV) of nearly 97°. These two elements can be reconfigured to perform beam steering switching or wavelength selection switching to dynamically establish communication links between the LCoS-AN and each TU in HANs. Fig. 1 shows a geometric room model [14] to demonstrate an applicable scenario for the proposed LCoS-AN techniques. This room model contains four identical LCoS-ANs which are connected directly to external optical fiber networks and several TUs, where each AN provides services for a specific coverage area inside the room. To demonstrate and prove the concept, a bidirectional optical wireless communication system at a transmission distance of 2.5 meters is experimentally implemented to evaluate the performance of the proposed LCoS-AN architecture. The experimental results show that the bit error ratios (BERs) of all transmitted channels (wavelengths) in both uplink and downlink transmissions are less than 10^{-9}.

2. Design of Node Architecture and Optical Terminal

The fundamental role of the proposed LCoS-AN is to exchange optical wavelengths between external fiber networks and indoor TUs without performing optical/electrical/optical (O/E/O) conversions. In this technique, a wide FOV of nearly 97 degrees can be achieved through the design of an LCoS-SLM that combines with a static diffraction grating element. As illustrated in Fig. 2, the pro-

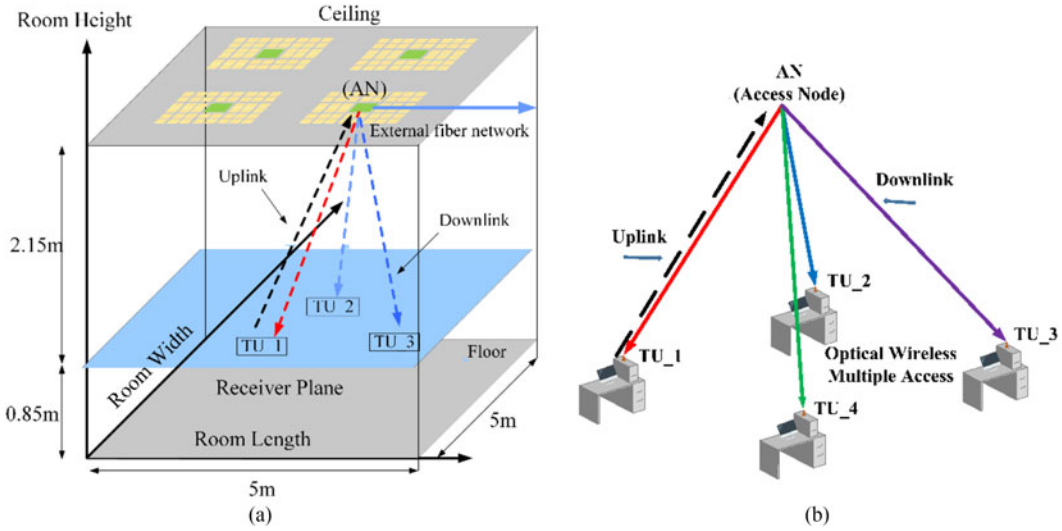

Fig. 1. Application of an LCoS-based access node in home area network (HAN). (a) Room model. (b) Specific coverage area for each AN.

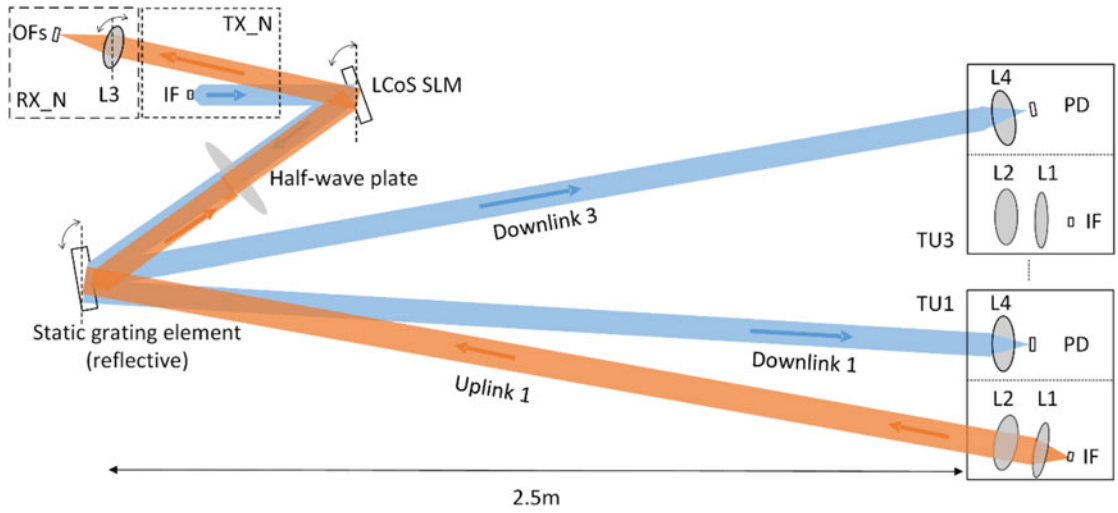

Fig. 2. Ray tracing of proposed node architecture in up/down link.

posed LCoS-AN consists of six major components including input fibers (IFs), output fibers (OFs), a lens for collimation (L3), a half-wave plate, a static diffraction grating element and an LCoS-SLM. The GRIN lens fiber is used as an IF medium for either downlink or uplink transmissions at the AN (TX_N) and each TU, respectively. The fiber ribbon, consisting of a row of 12 multimode fibers (62.5 um) which are based on a mechanically transferable (MT) connector with an inter-fiber spacing of 250 um, is used as the OFs at the AN's (RX_N) uplink receiver. In order to improve the fiber coupling efficiency in uplink transmission at AN (RX_N), a lens L3 is implemented in front of the fiber ribbon. A static diffraction grating element and an LCoS-SLM are used to perform wavelength selection switching or beam steering switching. Since these two elements are polarization sensitive, a half-wave plate is used to adjust the polarization property of incident light between these two elements. In TU, the GRIN lens fiber with a keplerian beam expander [15], which is composed by a pair of bi-convex lenses (L1 & L2), is used as the transmitter for uplink transmission. A receiver module, which is composed by a lens, L4 and a photodetector (PD), is used at TU to receive downlink optical

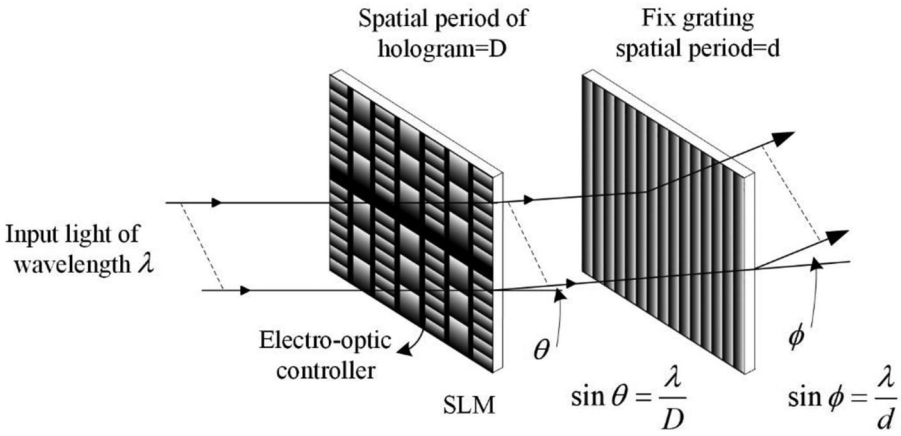

Fig. 3. Combination of a SLM and a static grating element.

signals from AN. The fundamental design principle of the AN and TU based on these components is described as follows:

2.1 Design of System Level Node Architecture

The design principle of the proposed LCoS-AN is based on the theory of diffraction grating. Multiple wavelengths contained in the incident beam of light are spatially separated by a diffraction grating element since each wavelength will be diffracted by the grating element at slightly different angles. Using a SLM instead of a static grating element allows one to have a programmable grating whose grating period can be varied as desired. The spatial separation of wavelengths can be converted from an angular separation if a lens is placed behind the programmable grating element. Another static diffraction grating element is used as usual in conjunction with the SLM since the used pixel pitch of SLM technology might be too large to obtain a desired grating period [16]. For wavelength selection based on the typical WDM channel plan with a spacing of 100 GHz, a wavelength separation of around 0.8 nm is essentially required in order to discriminate between different wavelengths. In this case, a pixel pitch of about 5 μm is required, which is beyond the technology development of current SLM [17]. Therefore, by introducing a static grating element of that order of spatial periodicity, the light can be angularly spread sufficiently to make a tuning resolution of about 0.8 nm. In this case, the SLM can be only operated to slightly change the diffraction angle of light, so allowing fine-tuning as illustrated by the concept in Fig. 3 [16]. Obviously a total diffraction angle of $\theta + \psi$ can be achieved, where the first angle, θ, is a variable for fine-tuning. The angle $\psi >> \theta$ is resulted from the reason that the static grating element has a fixed period. The order of combining SLM and static grating element can be varied, and as a result, an AN based on the use of this combination for bidirectional optical wireless communications can be designed. Although a passive beam-steering approach by employing a cascaded static reflection grating at the access point and wavelength tuning elements in the central communication controller has been experimentally demonstrated [18], [19], a tunable light source with a very wide tuning range should be used in order to diffract a wavelength to the desired position. Moreover, multiple tunable laser devices in parallel should also be employed to feed multiple wavelengths in the access point in order to simultaneously provide multiple beams for multiusers, which would not be cost-effective, and has difficulties to extend optical transport network directly since several repeated O/E/O conversions are required.

In the proposed LCoS-AN architecture, the LCoS-SLM is a vital component. It is reconfigurable because it is composed of optical phase array based on nematic liquid crystal (LC) materials, and is capable of displaying computer-generated holograms (CGHs) [20]. The device used in our

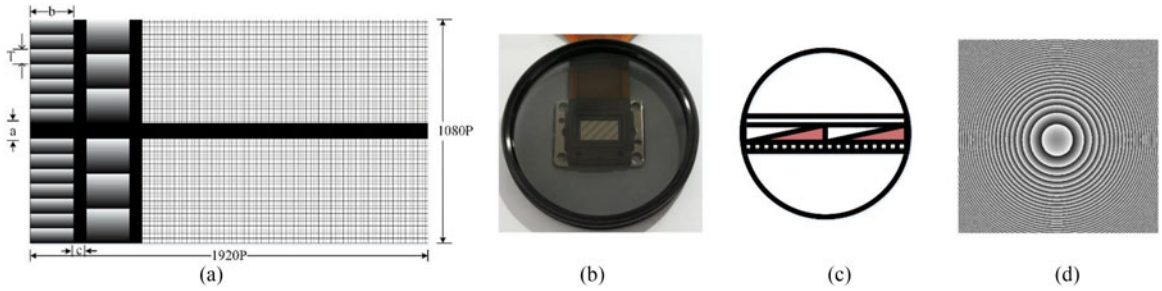

Fig. 4. Hologram design on LCoS device. (a). Design of sub-holograms on LCoS. (b). Typical hologram pattern shown on LCoS. (c). Multilevel-phase hologram based on a quantized blazed grating. (d). Multilevel-phase hologram based on a Fresnel lens function.

work is a test sample fabricated by an external foundry (JDC, Taiwan), which is composed of an array of 1920 $\times$ 1080 pixels. The filling factor is more than 0.93. The pixel pitch is 6.4 μm, leading to an active area that is diagonal of "0.7" with an aspect ratio of 16:9. The BL037 LC material (Merck, Germany) with a birefringence of $\Delta n = 0.216$ at 1550 nm was used to fill the device with homogeneous alignment by antiparallel rubbing on the alignment layer. Discretized voltages up to 256 levels between 0 and 10 V by using the DVI signal from a computer have been applied to control the states of liquid crystal on each pixel of the device. Therefore, the LCoS device is able to resolve 256 discrete modulation levels at a maximum phase depth of 2 π at 1550 nm. Due to the polarization-sensitive property of nematic LCoS device, the polarization property of incident light should be adjusted parallel to the director of LC materials in order to raise the efficiency of phase modulation.

In order to simultaneously conduct the wavelength selective switching and beam steering switching during both uplink and downlink transmissions, as illustrated in Fig. 4(a), the LCoS device is therefore sectioned into a top and a bottom half planes with a spacing of "a" pixels. Each half plane is further subdivided into several sub-planes in order to accommodate different holograms simultaneously. Each sub-plane is uploaded with a destined hologram (sub-hologram), where the width of each sub-hologram on the LCoS device is determined by the parameter "b". The parameter "c" represents the minimum spacing between two adjacent sub-holograms, and the parameter "T" is the period of sub-hologram. Except the hologram period, "T", it is obviously that a smaller "b" and "c" will result in a better utilization of LCoS device. The functionality of beam steering and wavelength routing from the node in uplink and downlink transmissions can be performed simultaneously, when different types of grating patterns (holograms) with different grating periods are designed and uploaded onto the LCoS devices. A typical phase hologram pattern is illustrated in Fig. 4(b) for reference. The designs of multilevel phase holograms based a quantized blazed grating and a Fresnel lens function are illustrated in Fig. 4(c) and (d), respectively.

2.2 Design of Terminal User (TU)

In the current research work of uplink transmission in OWC system, we assumes same wavelengths for each TU. However, when these wavelengths are simultaneously transmitted from multiple TUs, adjacent and co-channel interferences will be severe. Thus, in our design, each TU can transmit different wavelengths during uplink transmission. Although a tunable laser can be used as the light source to feed multiple wavelengths for TUs through optical fibers in our experiments, this setup for practical applications can be further improved for a low-cost configuration by using a broadband light source and a tunable filter such that each TU can arbitrarily choose a wavelength for uplink transmission. As illustrated in Fig. 2, each TU in our experiments is assumingly fabricated by using identical physical layer components for both transmitter and receiver modules. The transmitter module for uplink transmission consists of a GRIN lens fiber and a keplerian beam expander [15]

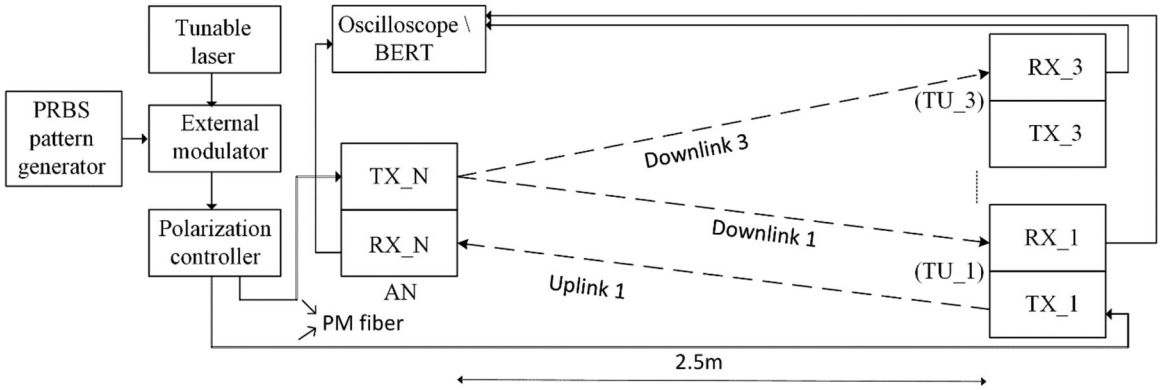

Fig. 5. Experimental setup of the bidirectional optical wireless communication links.

that is composed by a pair of bi-convex lenses (L_1 & L_2). The keplerian beam expander is designed to transmit optical wavelengths at a transmission distance of 2.5 m between the node and a TU. The separation distance of these two lens (L_1 & L_2) is equal to the sum of the focal lengths ($f_1 + f_2$). The beam size beyond the lens is determined by the beam properties at the end of fiber including the divergence, field distribution, and initial power [21]. Since the output field property of single-mode fibers is similar to a Gaussian profile [22], the output of beam expander can be analyzed through Gaussian beam propagation theory. The results show that the divergence angle, θ, beyond the beam expander can be calculated by:

$$\theta = \frac{2\lambda}{\pi w'}, \tag{1}$$

where λ is the wavelength and w' is the incident beam waist at the lens. It is obviously that a larger incident beam waist can reduce the divergence angle. Therefore, the beam expander can be designed to transfer a collimated beam of a small diameter D_1 into another collimated one of a larger diameter D_2:

$$D_2 = D_1 \times \frac{f_2}{f_1}. \tag{2}$$

The receiver module of TUs for receiving downlink transmission consists of a collimating lens (L_4) and a PD. The experimental setup for performance evaluation of LCoS-AN and TUs in the uplink and downlink transmissions are presented in the following sections.

3. Experimental Setup For Performance Evaluation

The LCoS-AN for bidirectional optical wireless communications was experimentally implemented by the setup of bidirectional transmission experiments in Fig. 5. In our experiments, a tunable laser (TL) capable of transmitting multiple wavelengths of spacing by 100 GHz at C band was used as the light source in both the uplink and downlink transmission experiments. All the lens and optical components used within the node and terminal architecture were purchased from the commercial market, and were stabilized on an optical breadboard through optomechanics, which were used to align and control the relative positions for experimental performance evaluation.

3.1 Uplink Transmission Setup

In the uplink transmission experiments to validate the concept, four typical WDM wavelengths (spaced by 0.8 nm and ranging from 1553.2 to 1555.6 nm) in C band, which were sequentially emitted from TL, were used as the light sources for each terminal user (TU), instead of using a

broadband light source and a tunable filter at each TU. These multiple wavelengths, which have been adjusted to the S polarization state from a polarization controller, were transmitted into a GRIN lens fiber (single mode fiber, SMF) as the transmitter of each TU through a polarization-maintaining (PM) SMF. The GRIN lens fiber has an operating wavelength of 1550 ± 30 nm and a working distance of 15 ± 5 mm. It is noted that the adjustment of polarization states of lights at TU is required because the static grating element (Newport, 1100 lines/mm), the first element of the node in uplink transmission, has a higher diffraction efficiency in the S polarization state. The light emitted from the GRIN lens fiber at each TU was fed into a pair of bi-convex lenses (L_1 & L_2), and delivered in free-space to the AN in uplink transmission. The focal lengths of these bi-convex lenses (L_1 & L_2) which serves as the keplerian beam expander, are 15 mm and 50 mm, respectively. The diameter of the light beam after being enlarged by the keplerian beam expander is around 1 mm, and the angle of divergence reduced by the expander is around 0.07 (deg.). The delivered optical wavelengths from each TU in uplink after transmitting to a distance of 2.5 m are diffracted by a static grating element before its incidence on the LCoS device. The static grating element converts these wavelengths into a different spatial separation, and thus each wavelength emerges from the static grating element at a slightly different angle. The static grating element was setup (52 degrees with respect to the vertical plane) to have an optimal grating efficiency in uplink transmission based on the fulfillment of the following specular reflection condition:

$$\theta_\alpha + \theta_\beta = 2\theta_G \tag{3}$$

where θ_α is the angle of incident light, θ_β is the 1st order diffraction angle, and θ_G is the blaze angle of the static grating. A half-wave plate placement between the static grating element and the LCoS device within the LCoS-AN was employed (22.5 degrees with respect to the optical axis) to adjust the polarization property of the lights such that the lights reaching each element can have a corresponding polarization state. The diffracted wavelengths from the static grating element were then steered to a desired fiber port of the output fiber ribbon by LCoS device (7.51 degrees with respect to the vertical plane). The control of LCoS device was performed through the upload of hologram patterns that have been designed. A quantized blazed grating pattern (for sub-hologram) based on the multilevel-phase LCoS SLM is shown in Fig. 4(c) where a grating period of nine pixels was used. For the wavelength of 1550 nm to fully switch between the output ports of the AN (i.e., port 1 $\sim$ port 4) in uplink transmission, a grating period of 45, 22, 14 and 9 pixels should be used, respectively. When different period of holograms is uploaded onto the LCoS device, we can therefore arbitrarily steer each wavelength to any desired output fiber port. A collimator (L_3), which has a focal length of 60 mm, was used in front of the output fiber ribbon to improve the coupling efficiency at the AN. In order to reduce light loss resulted from fiber coupling to be compatible with local area fiber networks, the multimode fibers were used as the output fibers in the AN but they can be connected to SMF-based fiber network through mode field adapters with very low light loss (less than 1 dB).

3.2 Downlink Transmission Setup

In the downlink transmission setup, four typical WDM wavelengths (channel spaced by 0.8 nm and ranging from 1550 to 1552.4 nm) in C band, which represents optical signals delivered from external fiber network, were launched down to the input fiber of the AN. The polarization state of these emitted wavelengths from TL was adjusted to be parallel to the director of LC materials (45 degrees), and was transmitted into a GRIN lens SMF as the transmitter within the AN through a PM SMF. The delivered lights from the GRIN lens fiber at AN were fed into the LCoS device. The LCoS device acts as a highly dispersive reflective phase grating element with a tunable period and pattern, which de-multiplexes the incident wavelengths and each wavelength, emerged from the LCoS device at slightly different angle. Each diffracted wavelength from LCoS is incident onto the different positions of the static grating element, which then converts these wavelengths into a spatial separation. By controlling the deflection angle of reflected beams from LCoS, the reflected beams from the static grating element can be routed to a TU as desired. The deflection angle of

LCoS-SLM depends on its displayed phase modulation pattern (hologram), where the maximum deflection angle for an LCoS-SLM with a pixel pitch of 6.4 um at 1550 nm can be calculated from the following equation:

$$\theta_d = \frac{\lambda}{\Delta} = \frac{1.55}{6.4} = 13.88 \text{ (degree)}. \tag{4}$$

Since a static grating element is used following the LCoS-SLM, the angular coverage (i.e., FOV) of the node in downlink transmission is therefore dominated by the maximum diffraction angle of the static grating element. In our experiments, a static grating element with a groove density of 1100 lines/mm has been used. The maximum diffraction angle of this grating from the node is roughly 96.8 degrees. The diffracted wavelengths delivered in free-space after being transmitted to a distance of 2.5 m were coupled into an InGaAs amplified PD (EOT, ET-3000A) through a collimating lens (L_4), which has a focal length of 15 mm, at the receiver module of TU. The PD used has a conversion gain of 1000 $\sim$ 1100 V/W between 1550 and 1600 nm. The active area diameter of this PD is 0.4 mm. In order to measure the performance of each diffracted wavelength, we can either move TU accordingly or steer each diffracted wavelength to the same TU through the control of LCoS-SLM.

In downlink transmission, the given multiple wavelengths delivered from external fiber networks to the AN is based on a time and wavelength division multiplexed (TWDM) configuration. The LCoS device can act as a focusing lens with its focal length adjustable in order to improve the alignment difficulty at each TU. In this experiment, the pattern of the focusing lens function is shown in Fig. 4(d), where each level of the gray color is the phase level of the LCoS, and was uploaded to LCoS device. Instead of acting as a highly dispersive phase grating element, the LCoS device acts as a dynamic lens. The focal length of the dynamic lens can be determined by:

$$f_{\text{LCoS}} = \frac{R_n^2}{\lambda}, \tag{5}$$

where R_n is the radius of the circle. By controlling the lens's focal length, the spot size focused on the TU can be dynamically adjusted.

4. Results and Discussions

The performance has been evaluated from the experimental setups as previously mentioned in Section 3. Link alignments between the AN and each TU in our experiments were performed by an infrared CCD camera (Scintacor, CamIR), where the results of system light loss as well as digital transmission experiments are presented as follows:

4.1 Analysis of System Light Loss

The insertion losses, caused by each optical component that was used in the proposed LCoS-AN architecture, are the most important system light loss. Moreover, the diffraction efficiency of phase grating element and fiber coupling efficiency also are important factors of the entire system loss. In our experiments, the insertion losses of each optical component used in the proposed LCoS-AN architecture were measured by using a standard power meter (Thorlabs PM100D). The total insertion losses of the TU in uplink transmission are 0.33 dB which is resulted from the GRIN lens fiber collimator (0.07 dB) and the pair of lenses L_1 & L_2 (0.11 dB and 0.15 dB).

The theoretical diffraction efficiency of the static grating element specified by the manufacturer is over 90% [23]. The measurement results show that only 71% has been achieved from the proposed node architecture in the optimal uplink transmission setup, which indicates a light loss of 1.82 dB from the uplink experiments. Its efficiency further degrades to 47.75% in the downlink transmission as the incident light is incident from an opposite direction, and indicates a light loss of 3.21 dB in the downlink experiments. The light loss resulted from the half-wave plate placement between the static grating element and the LCoS device was measured to be 2.07 dB and 1.96 dB in the

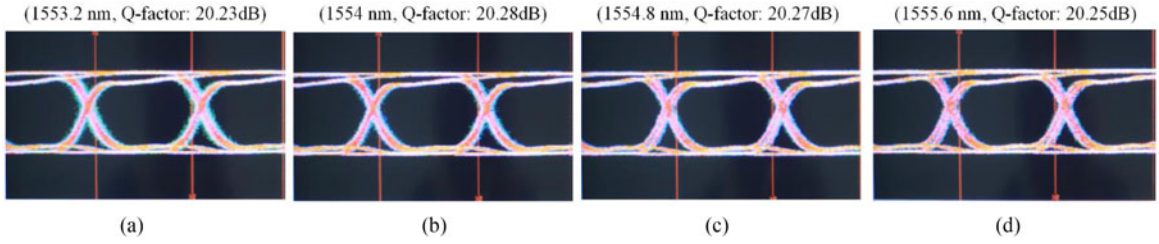

Fig. 6. Multiple wavelengths switched sequentially to the same output port of the node in uplink. (Port 3).

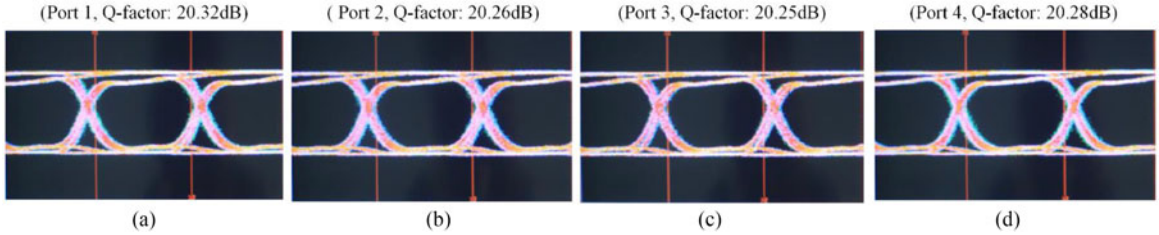

Fig. 7. Single wavelength switched sequentially to output ports of the node in uplink. ($\lambda = 1555.6$ nm).

uplink and downlink transmissions, respectively. The insertion loss of LCoS device was measured under the conditions of no uploaded diffraction grating patterns, where a loss of 1.91 dB in both transmission links was obtained. The diffraction efficiency of LCoS-SLM is calculated as the $+1$st diffraction order power relative to the 0th diffraction order power when no diffraction patterns are uploaded to the LCoS device. The measurement results show that the diffraction efficiency of LCoS SLM ranges from 17% to 36% in both uplink and downlink experiments. Therefore, a light loss of ranging from 4.3 to 7.4 dB was measured. The poor efficiency of the LCoS-SLM is attributed to the reason that the maximum modulation depth of phase in the LCoS device is smaller than 2 π, which has further caused the reduction of diffraction efficiency [24]. Moreover, the fringing effect between adjacent pixels, the imperfect phase profile of the varied layer thickness of LC and the non-uniformity of phase retardance on LCoS device may also cause its efficiency reduction [25], [26].

In the uplink experiments, a collimating lens, L_3, was placed in front of the output fiber array of the proposed LCoS-AN architecture to improve the fiber coupling efficiency. Therefore, an insertion loss of 0.12 dB $\sim$ 0.16 dB was measured. The coupling efficiency in each output fiber port of the node may vary since each wavelength at a desired output fiber port has different grating efficiency, physical offset and alignment error. Although the light loss resulted from the fiber coupling ranges from 5.2 to 6.67 dB, it can however be further improved by using a microlens array setup in front of the fiber ribbon according to our simulation results. The poor fiber-coupling problem can be omitted in the downlink experiments at the TU by using the collimating lens, L_4 with a PD as the receiver which only has an insertion loss of 0.17 dB in our measurements.

By measuring the insertion losses of all components in our experiments, we estimate that the system light losses in the uplink and downlink transmissions are roughly 15.82 dB $\sim$ 20.42 dB and 11.68 dB $\sim$ 14.76 dB, respectively. The crosstalk between adjacent channels of output fiber ports at AN is around -32 dB $\sim$ -42 dB according to the measurement results.

4.2 Digital Data Transmission Experiments

In order to explore the transmission characteristics of the proposed node architecture, the performances were evaluated in both scenarios of downlink and uplink transmissions by a LOS configuration. Although it is sufficient for each TU to use only a wavelength for uplink transmission, each TU needs to transmit different wavelengths in order to avoid adjacent and co-channel interferences.

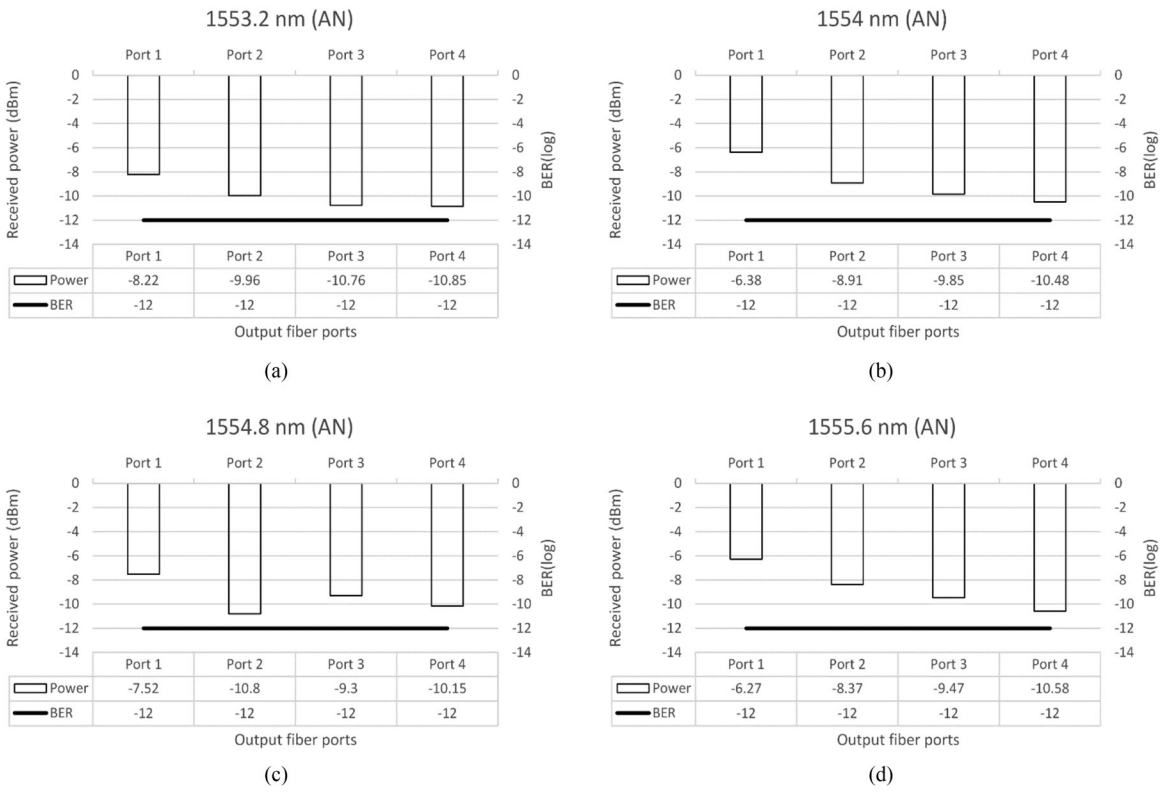

Fig. 8. Received power (AN) & BERs in uplink transmission.

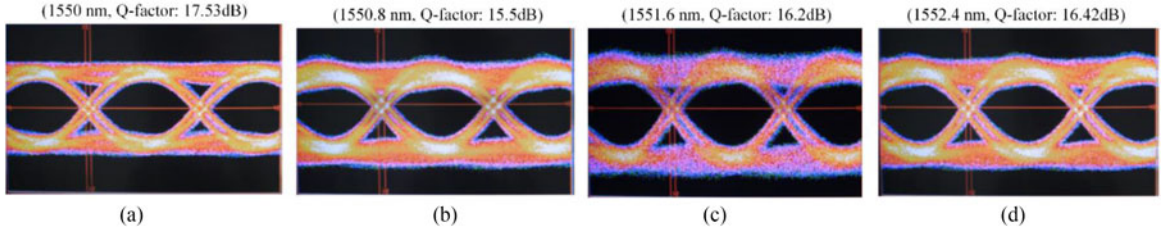

Fig. 9. Multiple wavelengths transmitted sequentially to a TU at different position in downlink.

Therefore, in the uplink transmission, multiple wavelengths transmitted sequentially from a TU were received by the AN, and each wavelength was then switched to a desired output fiber port of the fiber ribbon at the AN before it is delivered to an external optical fiber network. On the other hand, in downlink transmission, multiple wavelengths delivered from external optical fiber networks were transmitted through AN to TUs. Each wavelength can be transmitted to same or different TUs inside the coverage area of the AN approximately by a radius of 1.45 m. In the initial setup of the digital data transmission experiment at a data rate of 2.5 Gbps, a pulse pattern generator (Keysight N4970A) was used to generate a non-return-to-zero (NRZ) pseudo-random bit sequence (PRBS) of length $2^7 - 1$. These electrical signals were converted to optical signals through a tunable laser (TL) and an external Lithium Niobate Electro-Optic Modulator (10 Gbits/s, Agere Systems Inc.) that were used as the signal source of the transmitter in both uplink and downlink communication scenarios. The bit error ratios (BERs) of the digital transmission tests were estimated directly from

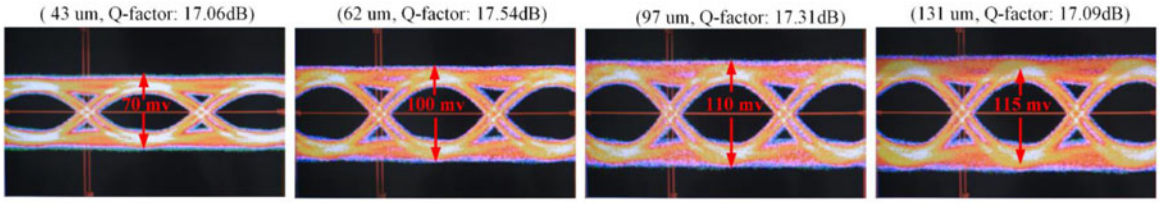

Fig. 10. Adjustable spot sizes focused at the same TU in downlink. (43 *um* to 131 *um*, $\lambda = 1550$ nm)

the Q factors [27]–[29] according to the measured eye diagrams by:

$$\mathrm{BER} = \frac{1}{2}\mathrm{erfc}\left(\frac{\mathrm{Q}}{\sqrt{2}}\right) \approx \frac{\exp\left(-\mathrm{Q}^2/2\right)}{\mathrm{Q}\sqrt{2\pi}}, \tag{6}$$

where the Q-factor is calculated by

$$\mathrm{Q} = \frac{I_1 - I_0}{\sigma_0 + \sigma_1} \tag{7}$$

with I_1 and I_0 being the means of the amplitude histograms at the logic one and zero levels, respectively. In (7), σ_0 and σ_1 are the standard deviations of the amplitude histograms at logic zero and one levels, respectively.

In the uplink transmission experiments, multiple wavelengths transmitted sequentially from a TU were received by the node and then switched to any port of the output fibers (i.e., port 1 $\sim$ port 4). The resulting eye diagrams for multiple wavelengths that were switched sequentially to the same output fiber port (i.e., port 3) are illustrated in Fig. 6 as a representative performance demonstration. According to the measured data (eye diagrams & histograms), the calculated Q-factors in dB ranges from 20.23 dB to 20.28 dB. The estimated BERs via the calculation from the Q-factors are all less than 10^{-12}. Moreover, each wavelength transmitted from the same TU can also be arbitrarily switched to any of the output fiber ports of the node. The measured eye diagrams for single wavelength sequentially switched to different fiber ports (i.e., port 1 $\sim$ 4) are illustrated in Fig. 7 as a representative performance demonstration. According to the measured data (eye diagrams & histograms), the calculated Q-factors in dB ranges from 20.25 dB to 20.32 dB. The estimated BERs calculated from the Q-factors are all less than 10^{-12}. The received powers at each output fiber port of the AN compared with the BERs are shown in Fig. 8.

In the downlink transmission experiments, multiple wavelengths delivered from optical input fiber (as representative optical signals from external fiber networks) were transmitted through the AN to TUs. The performance of multiple wavelengths transmitted to different TU, which was located at a slightly different position, has also been compared as shown by the representative illustration of performance in Fig. 9, where the calculated Q-factors in dB from the measured data (eye diagrams & histograms) are in a range of 15.5 dB and 17.53 dB. The estimated BERs calculated from Q-factors are all less than 10^{-9}. During this experiment, the spot sizes focused at a chosen TU (after the collimating lens, L_4) were investigated in order to improve the alignment difficulty at the TU. The spot sizes (defined by the radius of the $1/e^2$ contour), expanded from 43 to 131 *um* with respect to the setup of the LCoS, were measured by using knife-edge method [30] before the digital data transmission. The measured eye diagrams of single wavelength are shown by the representative illustration of performance in Fig. 10. According to the measured data (eye diagrams & histograms), the calculated Q-factors in dB are in the range of 17.06 dB and 17.54 dB. The estimated BERs as calculated from Q-factors are all less than 10^{-9}. The reason that the calculated Q-factors from uplink are higher than that from downlink is attributed to the higher transmitted power in uplink that is 10 dBm in comparison to 9.5 dBm in downlink. However, these launched powers are all within the eye-safety limit according to the accessible emission limit (AEL) estimated at 2.5 m distance, which is about 10.18 dBm [19], [31]. The system performance has also further verified through a

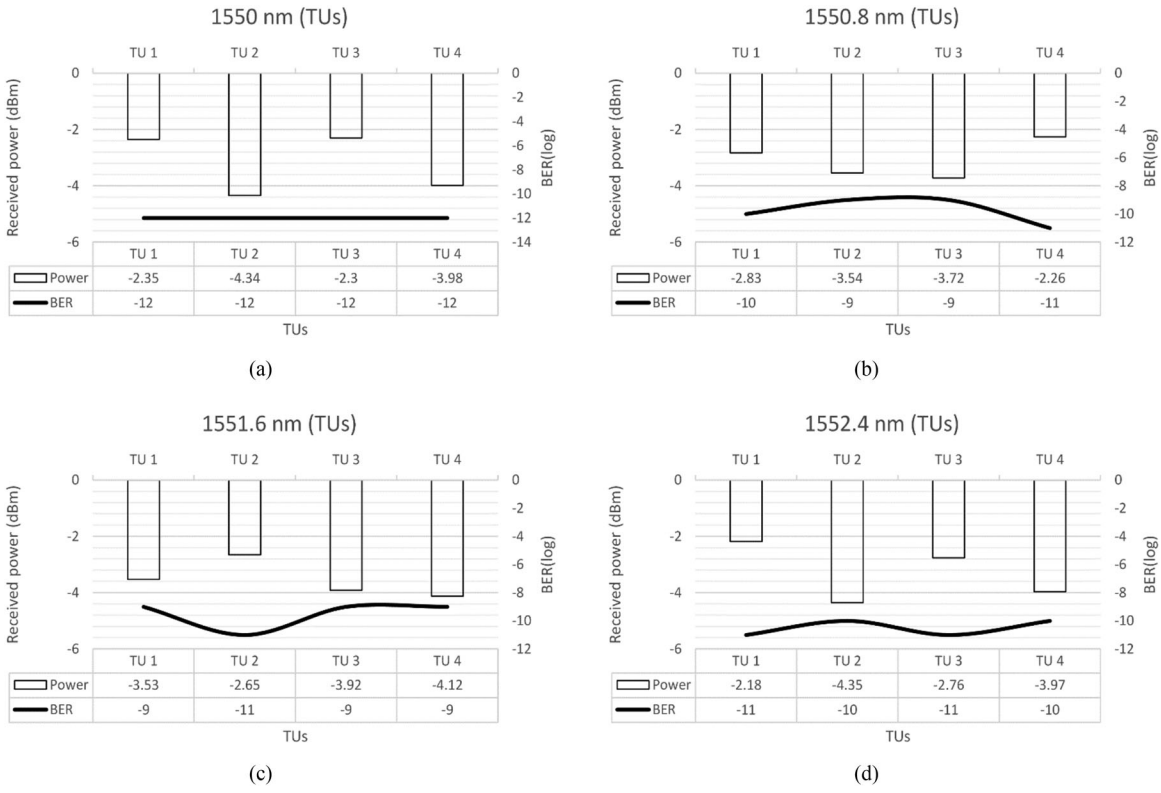

Fig. 11. Received power (TUs) & BERs in downlink transmission.

BERT (BER tester) and the measured BERs are all less than 10^{-9}. The received powers at each TU compared with the BERs are shown in Fig. 11.

5. Conclusion

This paper reports the design of an LCoS-AN architecture using optical fibers as the transmitter and receiver to exchange multiple wavelength transmissions between external fiber networks and indoor terminal users without performing any O/E/O conversion. The experimental results of system level evaluation, which was based on the use of typical WDM wavelengths (channel spacing by 100 GHz), and modulated at a data rate over 2.5 Gbps at a transmission distance of 2.5 meters, show that the estimated BERs of all the wavelengths in both downlink and uplink transmission scenarios are all less than 10^{-9}. To the best of our knowledge, this is the first time, for the proof of concept, that an LCoS-based node architecture capable of wavelength selective switching and beam steering switching is experimentally implemented and demonstrated for indoor bidirectional optical wireless communication applications. Our work potentially provides an alternative key-enabling solution to deliver the high-speed data transmission from a local optical fiber network to a home area network through indoor bidirectional optical wireless communications.

References

[1] *ITU-T Recommendation G.989.1:40-Gigabit*-Capable Passive Optical Networ*ks (NG-PON2): General* R*equirements*, Int. Telecommun. Union, Geneva, Switzerland, 2015.
[2] D. Nesset, “NG-PON2 technology and standards,” *J. Lightw. Technol.*, vol. 33, no. 5, pp. 1136–1143, Mar. 2015.

[3] K. D. Langer and J. Vučić, "Optical wireless indoor networks: Recent implementation efforts," in *Proc. 36th Eur. Conf. Exhib. Opt. Commun.*, Torino, Italy, 2010, pp. 1–6.

[4] M. A. Khalighi and M. Uysal, "Survey on free space optical communication: A communication theory perspective," *IEEE Commun. Surveys Tut.*, vol. 16, no. 4, pp. 2231–2258, Fourthquarter 2014.

[5] J. M. Kahn and J. R. Barry, "Wireless infrared communications," *Proc. IEEE*, vol. 85, no. 2, pp. 265–298, Feb. 1997.

[6] A. G. Al-Ghamdi and J. M. H. Elmirghani, "Spot diffusing technique and angle diversity performance for high speed indoor diffuse infra-red wireless transmission," *IEE Proc.Optoelectron.*, vol. 151, no. 1, pp. 46–52, 2004.

[7] F. E. Alsaadi and J. M. H. Elmirghani, "Adaptive mobile line strip multibeam MC-CDMA optical wireless system employing imaging detection in a real indoor environment," *IEEE J. Sel. Areas Commun.*, vol. 27, no. 9, pp. 1663–1675, Dec. 2009.

[8] F. E. Alsaadi and J. M. H. Elmirghani, "Performance evaluation of 2.5 Gbit/s and 5 Gbit/s optical wireless systems employing a two dimensional adaptive beam clustering method and imaging diversity detection," *IEEE J. Sel. Areas Commun.*, vol. 27, no. 8, pp. 1507–1519, Oct. 2009.

[9] H. L. Minh *et al.*, "A 1.25-Gb/s indoor cellular optical wireless communications demonstrator," *IEEE Photon. Technol. Lett.*, vol. 22, no. 21, pp. 1598–1600, Nov. 2010.

[10] K. Wang, A. Nirmalathas, C. Lim, and E. Skafidas, "4x 12.5 Gb/s WDM optical wireless communication system for indoor applications," *J. Lightw. Technol.*, vol. 29, no. 13, pp. 1988–1996, Jul. 2011.

[11] F. Feng, I. H. White, and T. D. Wilkinson, "Free space communications with beam steering a two-electrode tapered laser diode using liquid-crystal SLM," *J. Lightw. Technol.*, vol. 31, no. 12, pp. 2001–2007, Jun. 2013.

[12] A. Gomez *et al.*, "Beyond 100-Gb/s indoor wide field-of-view optical wireless communications," *IEEE Photon. Technol. Lett.*, vol. 27, no. 4, pp. 367–370, Feb. 2015.

[13] H.-H. Chou and J. Hsiao, "LCoS-based access node for bidirectional optical wireless communications," in *Proc. Opt. Fiber Commun. Conf.*, 2018, Paper M1F.7.

[14] L. Zeng *et al.*, "High data rate multiple input multiple output (MIMO) optical wireless communications using white led lighting," *IEEE J. Sel. Areas Commun.*, vol. 27, no. 9, pp. 1654–1662, Dec. 2009.

[15] H. Y. Hsu, W. C. Lu, H. L. Minh, Z. Ghassemlooy, Y. L. Yu, and S. K. Liaw, "2 $\times$ 80 Gbit/s DWDM bidirectional wavelength reuse optical wireless transmission," *IEEE Photon. J.*, vol. 5, no. 4, Aug. 2013, Art. no. 7901708.

[16] M. C. Parker, A. D. Cohen, and R. J. Mears, "Dynamic digital holographic wavelength filtering," *J. Lightw. Technol.*, vol. 16, no. 7, pp. 1259–1270, Jul. 1998.

[17] Z. Zhang, Z. You, and D. Chu, "Fundamentals of phase-only liquid crystal on silicon (LCOS) devices," *Light Sci. Appl.*, vol. 3, 2014, Art. no. e213.

[18] A. M. J. Koonen, C. W. Oh, and E. Tangdiongga, "Reconfigurable free-space optical indoor network using multiple pencil beam steering," in *Proc. OptoElectron. Commun. Conf. Aust. Conf. Opt. Fibre Technol.*, Melbourne, VIC, Australia, 2014, pp. 204–206.

[19] C. W. Oh, Z. Cao, E. Tangdiongga, and T. Koonen, "Free-space transmission with passive 2 D beam steering for multigigabit-per-second per-beam indoor optical wireless networks," *Opt. Exp.*, vol. 24, pp. 19211–19227, 2016.

[20] Z. Zhang *et al.*, "High quality assembly of phase-only liquid crystal on silicon (LCOS) devices," *J. Display Technol.*, vol. 7, no. 3, pp. 120–126, 2011.

[21] P. LoPresti, H. Refai, and J. Sluss, "Adaptive power and divergence to improve airborne networking and communications," in *Proc. 24th Digit. Avionics Syst. Conf.*, Washington, DC, USA, 2005, pp. 1.B.1–1.1–6.

[22] B. Yang, J. Duan, Z. Xie, and H. Xiao, "Evaluation of mode field diameter of step-index fibers and comparison analysis," *RES J. Appl. Sci., Eng. Technol.*, vol. 6, no. 3, pp. 382–386, 2013.

[23] 2016. [Online]. Available: https://www.newport.com/c/diffraction-gratings

[24] I. Moreno, C. Iemmi, A. Márquez, J. Campos, and M. J. Yzuel, "Modulation light efficiency of diffractive lenses displayed in a restricted phase-mostly modulation display," *Appl. Opt.*, vol. 43, no. 34, pp. 6278–6284, 2004.

[25] T. Lu, M. Pivnenko, B. Robertson, and D. Chu, "Pixel-level fringing-effect model to describe the phase profile and diffraction efficiency of a liquid crystal on silicon device," *Appl. Opt.*, vol. 54, no. 19, pp. 5903–5910, 2015.

[26] L. Teng, M. Pivnenko, B. Robertson, R. Zhang, and D. Chu, "A compensation method for the full phase retardance nonuniformity in phase-only liquid crystal on silicon spatial light modulators," *Opt. Exp.*, vol. 22, no. 21, pp. 26392–26402, 2014.

[27] G. P. Agrawal, *Lightwave Technology Telecommunication System.* Hoboken, NJ, USA: Wiley, 2005.

[28] F. Zhang, H.-H. Chou, and W. A. Crossland, "PLZT-based shutters for free-space optical fiber switching," *IEEE Photon. J.*, vol. 8, no. 1, Feb. 2016, Art. no. 7800512.

[29] N. Dong-Nhat, M. A. Elsherif, and A. Malekmohammadi, "Investigations of high-speed optical transmission systems employing Absolute added correlative coding (AACC)," *Opt. Fiber Technol.*, vol. 30, pp. 23–31, 2016.

[30] D. Wright, P. Greve, J. Fleischer, and L. Austin, "Laser beam width, divergence and beam propagation factor -and international standardization approach," *Opt. Quantum Electron.*, vol. 24, pp. S993–S1000, 1992.

[31] *International Standard IEC 60825—1 IEC: 1993 + A1:1997 + A2:2001: Safety of Laser Products—Part 1:Equipment Classification and Requirements.* Int. Electrotech. Commissions, Geneva, Switzerland, 2001.